

**Machine learning in orthodontics:
Introducing a 3D auto-segmentation and auto-landmark finder of CBCT
images to assess maxillary constriction in unilateral impacted canine
patients**

Si Chen^a; Li Wang^b; Gang Li^c; Tai-Hsien Wu^d; Shannon Diachina^e; Beatriz Tejera^f; Jane Jungeun Kwon^e; Feng-Chang Lin^g; Yan-Ting Lee^e; Tianmin Xu^h; Dinggang Shenⁱ; Ching-Chang Ko^j

ABSTRACT

Objectives: To (1) introduce a novel machine learning method and (2) assess maxillary structure variation in unilateral canine impaction for advancing clinically viable information.

Materials and Methods: A machine learning algorithm utilizing Learning-based multi-source IntegratiON framework for Segmentation (LINKS) was used with cone-beam computed tomography (CBCT) images to quantify volumetric skeletal maxilla discrepancies of 30 study group (SG) patients with unilaterally impacted maxillary canines and 30 healthy control group (CG) subjects. Fully automatic segmentation was implemented for maxilla isolation, and maxillary volumetric and linear measurements were performed. Analysis of variance was used for statistical evaluation.

Results: Maxillary structure was successfully auto-segmented, with an average dice ratio of 0.80 for three-dimensional image segmentations and a minimal mean difference of two voxels on the midsagittal plane for digitized landmarks between the manually identified and the machine learning-based (LINKS) methods. No significant difference in bone volume was found between impaction ($[2.37 \pm 0.34] \times 10^4 \text{ mm}^3$) and nonimpaction ($[2.36 \pm 0.35] \times 10^4 \text{ mm}^3$) sides of SG. The SG maxillae had significantly smaller volumes, widths, heights, and depths ($P < .05$) than CG.

Conclusions: The data suggest that palatal expansion could be beneficial for those with unilateral canine impaction, as underdevelopment of the maxilla often accompanies that condition in the early teen years. Fast and efficient CBCT image segmentation will allow large clinical data sets to be analyzed effectively. (*Angle Orthod.* 2020;90:77–84.)

KEY WORDS: Machine learning; CBCT; Canine impaction; Orthodontics; Image segmentation

^a Associate Professor, Department of Orthodontics, Peking University School and Hospital of Stomatology, PR China; and Visiting Scholar, Oral and Craniofacial Health Sciences Research, School of Dentistry, University of North Carolina, Chapel Hill, NC.

^b Assistant Professor, Department of Radiology; and Biomedical Research Imaging Center School of Medicine, University of North Carolina, Chapel Hill, NC.

^c Assistant Professor, Biomedical Research Imaging Center, School of Medicine, University of North Carolina, Chapel Hill, NC.

^d Postdoctoral Researcher, Oral and Craniofacial Health Sciences Research, School of Dentistry, University of North Carolina, Chapel Hill, NC.

^e Research Assistant, Oral and Craniofacial Health Sciences Research, School of Dentistry, University of North Carolina, Chapel Hill, NC.

^f Dental Student, Oral and Craniofacial Health Sciences Research, School of Dentistry, University of North Carolina, Chapel Hill, NC.

^g Associate Professor, Department of Biostatistics, University of North Carolina, Chapel Hill, NC.

^h Professor, Department of Orthodontics, Peking University School and Hospital of Stomatology, PR China.

ⁱ Professor, Department of Radiology; and Director, Biomedical Research Imaging Center, School of Medicine, University of North Carolina, Chapel Hill, NC.

^j Professor, Oral and Craniofacial Health Sciences Research; and Chair, Department of Orthodontics, School of Dentistry, University of North Carolina, Chapel Hill, NC.

Corresponding author: Dr Ching-Chang Ko, School of Dentistry, Department of Orthodontics, 275 Brauer Hall, CB# 7450, Chapel Hill, NC 27599

(e-mail: Ching-Chang_Ko@unc.edu)

Accepted: May 2019. Submitted: January 2019.

Published Online: August 12, 2019

© 2020 by The EH Angle Education and Research Foundation, Inc.

INTRODUCTION

Machine learning is a branch of artificial intelligence that uncovers patterns in data automatically and then applies the detected patterns for future data prediction or decision making.¹ This field has exploded in development as a result of rapid increases in computer storage capacity and processing power, thereby allowing for the application of machine learning in medical diagnosis, bioinformatics, robotics, and more.² Although applications within dentistry, and particularly orthodontics, are in their infancy, artificial intelligence shows potential for use in orthodontics for diagnosis of tooth extraction and evaluation of facial attractiveness.³ The goal of this study was twofold: (1) introduction of advanced machine learning–based imaging technologies and, for the first time, utilization of these technologies for (2) characterization of three-dimensional (3D) skeletal variations in orthodontic patients with impacted maxillary canines.

Maxillary canines are the second most frequently impacted teeth, following mandibular third molars.⁴ The prevalence of maxillary canine impaction is approximately 2% in the general population,⁵ and 83%–92% of all impacted maxillary canine cases are unilateral impactions.⁶ While the exact etiology is unknown, it has been proposed⁷ that localized, systemic, or genetic etiologic factors contribute to canine impaction. Because maxillary canines have the longest duration of development in the deepest area of the maxilla, followed by the longest and most tortuous path of eruption,⁸ skeletal maxillary structure variation may be either an etiologic factor affecting canine eruption or a result of underdevelopment of the maxilla.

Previous studies measured linear length of the transverse dimension of the maxilla, which could not fully describe the 3D volumetric morphology. By analyzing the radiographs of unilateral impacted canine subjects, Al-Khateeb et al.⁹ reported that the transverse maxillary width on the impaction side was larger than on the nonimpaction side. Conversely, Yan et al.¹⁰ analyzed cone-beam computed tomography (CBCT) scans of subjects with impacted canines, finding the maxillary dental and skeletal widths to be significantly smaller in subjects with buccally impacted canines. CBCT can provide essential information in the preoperative assessment of a volumetric estimate for canine occupancy, as well as in pathway evaluation for orthodontic guided canine eruption. However, previous work with CBCT image analysis has relied on human raters to manually draw the region of interest point by point based on the intensity rendering. Cevidanes et al.¹¹ applied ITK-SNAP,¹² an interactive software application that allows users to navigate 3D medical images, to manually delineate anatomical regions of

Table 1. The Demographic Distributions of Study Group and Control Group^a

	Study Group	Control Group
No. of application samples	30	30
Female, n (%)	12 (40)	18 (60)
Mean age \pm SD, y	14.97 \pm 2.04	14.53 \pm 2.24
Age range, y	11–18	11–18
No. of buccal, n (%)	16 (53)	N/A
No. of mid-alveolus, n (%)	4 (13)	N/A
No. of palatal, n (%)	10 (33)	N/A

^a SD indicates standard deviation; N/A, not applicable.

interest and perform semiautomatic CBCT segmentation. The method is still tedious, time-consuming, and user-dependent, leading to a technical bottleneck inhibiting widespread clinical implementation.

Automatic methods for accurate estimation of the maxillary volume and its architecture are lacking, particularly with regard to 3D volumetric characterization of impacted canine patients. By introducing a novel machine learning algorithm, Learning-based multi-source IntegrationN framework for Segmentation (LINKS),¹³ this study aims to quantify the volumetric discrepancy of the skeletal maxilla in a Chinese population with unilaterally impacted maxillary canines while overcoming the image auto-segmentation and postprocessing obstacles currently being faced for clinical application. It was hypothesized that variation in maxillary structure has a role in unilateral canine impaction, with potential maxillary underdevelopment occurring in impaction patients.

MATERIALS AND METHODS

Pretreatment CBCT data for 145 consecutive subjects were collected from Peking University Hospital with institutional ethical committee approval (IRB: PKUSSIRB-201626016). CBCTs were routinely acquired to avoid iatrogenic root resorption and other tissue damage. Among those, 107 CBCT images with good quality were chosen, of which 36 CBCTs were randomly selected as training samples (also known as “ground truth”) and test samples. The remaining 71 CBCTs were further filtered to 60 CBCTs and clustered into two groups: a study group (SG) of 30 subjects with clinically diagnosed unilateral maxillary canine impactions and an age-matched control group (CG) of 30 subjects without impacted canines. The demographic distributions were similar between the two groups, as shown in Table 1. The exclusion criteria for the study group included (1) previous orthodontic treatment, (2) bilateral maxillary canine impaction, (3) combined incisor and canine impactions, (4) cleft palate or other maxillofacial syndromes, (5) maxillary dental/skeletal trauma or surgical history, and (6) dental age younger

than the late mixed dentition. The same exclusion criteria were applied to the control group.

The CBCT machine (NewTom VG, QR s.r.l., Verona, Italy) was used under the following settings: 15×15 -cm field of view, 110 kV, and 1–20 mA (pulsed mode) with a resolution of 0.3 mm isotropic voxel and exposure time of 10 seconds.

Maxilla Auto-segmentation

LINKS, based on advanced machine learning imaging techniques by Wang et al. in 2016,¹³ was utilized to auto-segment the maxilla. Generally, there are three stages in a machine learning application: a preparation stage, a training and test stage, and an application stage.

Preparation stage. Thirty-six CBCT images were manually segmented using the software, ITK-SNAP¹² to isolate the maxilla and mandible. These manually segmented CBCTs with labeled objects were used for training and testing in the following stage.

Training and test stage. All manually segmented CBCTs (36 scans) were divided into two subsets: a training set (30 scans) and a test set (six scans). In the training stage, a majority voting strategy was employed to generate the initial segmentation probability maps of the maxilla and mandible. Specifically, all of the training samples were aligned onto a training sample by affine registration, and a majority voting at each voxel was implemented to generate the probability maps of the maxilla and mandible.¹³ Features from these probability maps and the 30 CBCTs in the training set provided important learning guidance for CBCT segmentation. LINKS used the random forest method.¹³ Briefly, 10 sequential random forest classifiers were calculated from the features vectors and the training set. These classifiers allowed determination of numerous image features for the most suitable, accurate CBCT auto-segmentation. In addition, the segmentation probability map was updated sequentially after applying the classifiers. In the test stage, the majority voting strategy was also employed to calculate the initial segmentation probability maps of the maxilla and mandible of CBCT scans in the test set. Then, the learned classifiers were sequentially applied to iteratively refine these probability maps of test samples.

The automatically segmented results were compared to the manually segmented results to estimate the accuracy of the learned classifiers. The Dice ratio is the most used metric in validating volumetric segmentation of medical images. Its definition is given as follows:

$$Dice = \frac{2|A \cap B|}{|A| + |B|},$$

where $|A|$ and $|B|$ represent the cardinalities of the learned and manual sets, and $|A \cap B|$ represents the intersection of the two sets. A value of 0 indicates no similarity, whereas a value of 1 indicates perfect agreement.

Application stage. Similar to the process in the test stage, the majority voting strategy was used to estimate the initial segmentation probability maps of the maxilla and mandible of the unlabeled application samples, and then the learned classifiers were sequentially applied to iteratively refine these probability maps. The flowchart of the entire automatic segmentation method using the machine learning method is shown in Figure 1.

Midsagittal Plane Construction

To assess maxillary asymmetry, a midsagittal plane was constructed. The basion (Ba), nasion (Na), and anterior nasal spine (ANS) landmarks were automatically digitized for each sample using the aforementioned similar algorithm.¹⁴ The proposed locations of these landmarks in the sagittal, coronal, and horizontal views in the training set were manually identified for learning (Figure 2). The midsagittal plane was defined as the plane passing through the Ba, Na, and ANS landmarks. This resultant plane was used to divide the maxillary segmentation into halves for analysis of unilateral canine impaction. The automatically digitized landmarks were validated by comparing them with the manually defined landmarks in CBCT images in the test set.

Superimposition

For the study group, the impaction side of the maxilla was converted to surface mesh and mirrored to the surface mesh of the nonimpaction side, followed by superimposition. The geometric difference between a vertex and its closest corresponding vertex on the flipped surface mesh of the impaction side was computed and visualized on a color map for three impaction types (buccal, mid-alveolus, and palatal).

Volumetric, Width, Height, and Depth Measurement of the Maxilla

Volumetric measurements for the two maxillary halves were performed by voxel counts. Measurements were divided into impaction and nonimpaction sides for the SG for comparison. Total volumetric differences between the CG and SG were compared. In addition, three linear measurements (maxillary width, height, and depth) were compared between the two groups. The definition of the maxillary width was a distance measured between left and right jugular

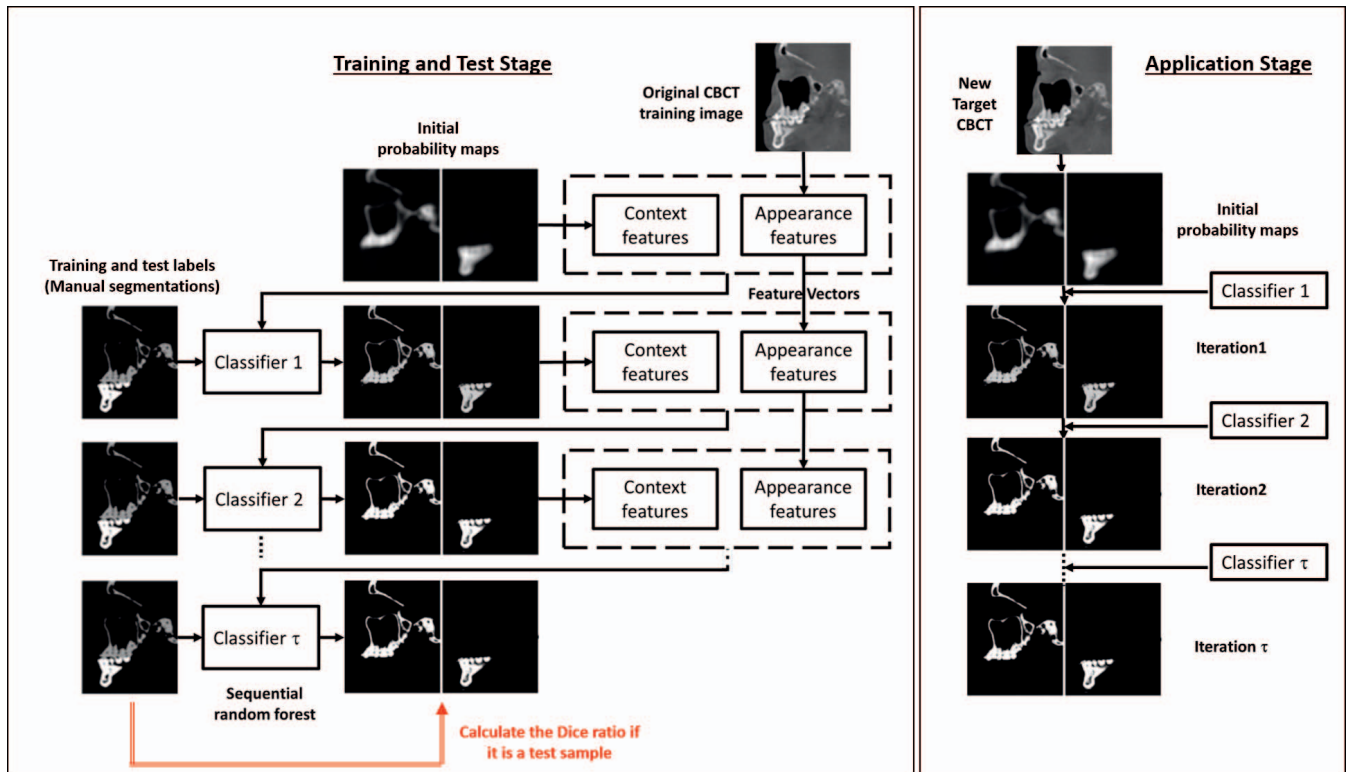


Figure 1. Flowchart of the automatic segmentation method. In the training stage (left), a series of sequential random forest classifiers were obtained through iterative training using the appearance features from the original CBCT, the context features from the updated segmentation probability maps, and the training labels. In the application stage (right), these classifiers were sequentially applied to the new target CBCT to iteratively generate the final segmentation.

points; the maxillary height was defined as a distance measured between the most superior border of the frontal process of the maxilla and the most inferior point of alveolar process; and the maxillary depth was defined by a distance measured from ANS to a point directly posterior to ANS that was on the line drawn from the most distal boundaries of the right and left maxillary sinuses.

Statistical Analysis

Analysis of variance was used to compare the group differences in volume, width, height, and depth, with adjustments by sex and age using a linear model. The reliability of the machine learning algorithms was shown by intraclass correlation coefficients (ICCs), which were calculated based on three repeated prediction accuracies from six subjects.

RESULTS

Fully Automatic Maxilla Segmentation

Figure 3 illustrates an example of a final rendering of the segmented maxilla and mandible from a high-resolution machine (Hitachi Medical Corporation, Tokyo, Japan), which took approximately 1 hour. How-

ever, as a result of limited access, a lower resolution machine (NewTom VG, QR s.r.l.) regularly used for clinical application was implemented for the bulk of the segmentation. A final segmented maxilla from the lower resolution machine is shown in Figure 4A. The processing time of CBCT images with lower resolution was reduced to 15 minutes per CBCT image set using a single core of Intel Processor X5670. The program can be speeded up further by performing tasks on a more modern central processing unit (CPU) or by using parallel computing such as multi-core or graphics processing unit (GPU) computing.

Veracity of the Machine Learning and Superimposition

The average Dice ratio of the maxilla was 0.800 ± 0.029 , ranging from 0.742 to 0.830, proving excellent accuracy. The mean difference in voxel position between the manually identified and automatically digitized landmarks was 1.92 ± 1.02 for Ba, 2.23 ± 1.19 for Na, and 2.26 ± 1.38 for ANS (1 voxel = 0.3 mm). Reliability was further evaluated using ICC. The values of ICC were 0.994 and 0.999 for the auto-segmentation and auto-landmark results, respectively, which are highly reliable. Thus, the reliability of the

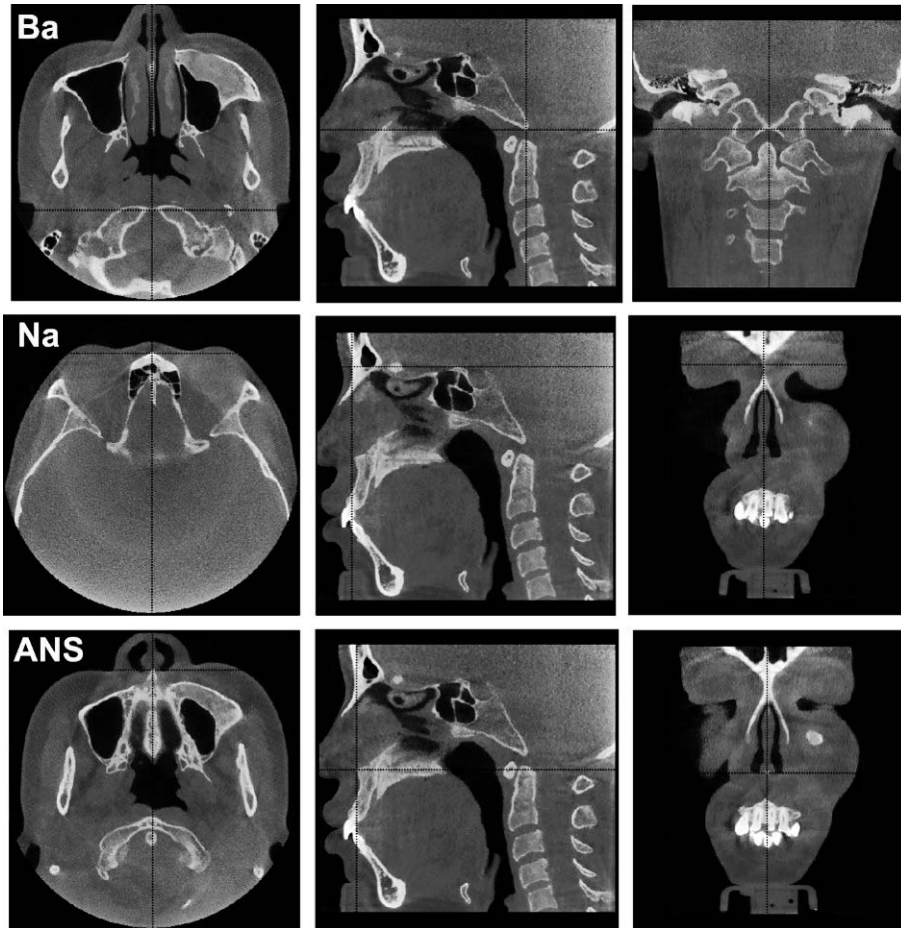


Figure 2. The proposed location of the three landmarks (Ba, Na, and ANS) used to define the midsagittal plane are shown by the cross-points of two black lines.



Figure 3. An example of automatic segmentation results. Per the study design, the craniofacial area was segmented into three regions of interest (ROIs): maxilla (yellow), mandible (red), and the rest of the craniofacial skeleton (blue).

algorithm was validated. The superimposition results of three different types of impaction (buccal, mid-alveolus, and palatal) are shown in Figure 4B. There was little geometric difference for the mid-alveolus impaction case, while the buccal impaction and the palatal impaction showed reasonably anatomic differences, specifically of the alveolar ridge at the canine eminence.

Clinical Outcomes

On average, the SG tended to have a smaller maxillary volume (5000 mm³ less) than the CG ($P = .006$), and the volume in males ($5.36 \pm 0.71 \times 10^4$ mm³) was significantly larger than in females ($4.59 \pm 0.44 \times 10^4$ mm³) ($P < .001$). The difference between SG ($4.73 \pm 0.67 \times 10^4$ mm³) and CG ($5.22 \pm 0.65 \times 10^4$ mm³) was still significant in volume, even after being adjusted for sex and age ($P = .023$). In the SG, the average volumes of the nonimpaction ($[2.36 \pm 0.35] \times 10^4$ mm³) and impaction sides ($[2.37 \pm 0.34] \times 10^4$ mm³) were not significantly different.

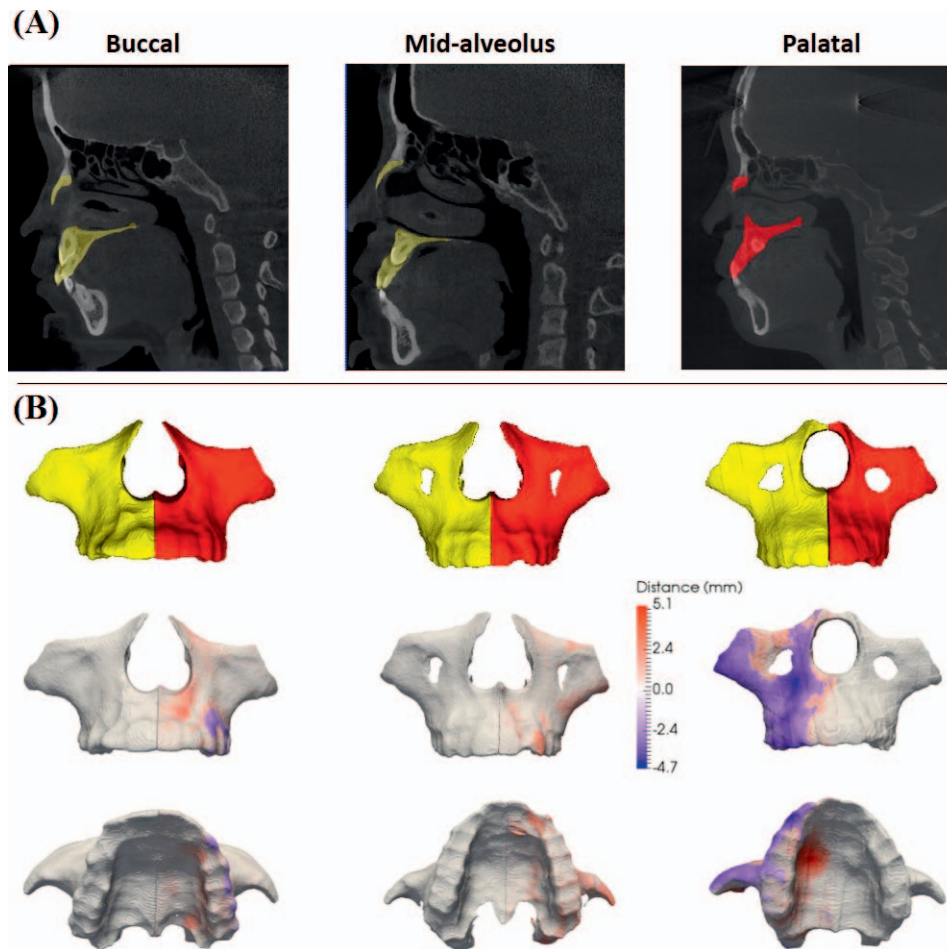


Figure 4. (A) Segmentation results for the maxilla. (B) The superimposition results of three different types of impaction (buccal, mid-alveolus, and palatal) are shown, allowing for geometric difference determination.

The averaged width, height, and depth in males (67.4 ± 4.4 , 67.1 ± 3.4 , and 50.8 ± 2.7 mm, respectively) were significantly greater than in females (63.5 ± 4.1 , 64.9 ± 3.6 , and 46.5 ± 3.0 mm, respectively) ($P = .002$, $P = .019$, and $P < .001$). The SG tended to have a smaller width, height, and depth than the CG, as shown in Table 2 (for width, 64.3 ± 5.3 mm [SG] and 66.6 ± 3.6 mm [CG], $P = .047$; for height, 65.1 ± 3.6 mm [SG] and 67.0 ± 3.5 mm [CG], $P = .049$; and for depth, 47.7 ± 3.6 mm [SG] and 49.6 ± 3.3 mm [CG], $P = .041$). The impaction effect in all dimensions became nonsignificant after being adjusted for age and gender.

DISCUSSION

The superimposition maps shown in Figure 4B represent the typical morphological discrepancy between the impaction and the nonimpaction maxillary halves, and they were consistent with Yan's finding¹⁰ of maxillary constriction for the canine impaction patients. The maps illustrate approximately 2.4 mm of trans-

verse constriction, which better agrees with the mean difference of 2.3 mm from all 30 SG subjects than with that of the 30 matched CG subjects. In clinic, the 2-mm constriction can be simply corrected by archwire expansion. Nevertheless, the volumetric constriction was found to be approximately 5000 mm^3 , which was five times that of a canine's volume. The data may explain O'Neill's finding,¹⁵ in which the use of rapid maxillary expansion in the early mixed dentition effectively increased the rate of eruption of palatally displaced maxillary canines compared to an untreated control group. Generation of such data that provides evidence for a clinical modality would have been impossible without this machine learning approach. Conventional radiographic studies are limited to linear measurements. Present technology has integrated 3D volumetric and two-dimensional linear measurements, allowing for assessment of craniofacial growth and orthodontic diagnosis and treatment.¹⁶ Future analysis will use a larger data set with extensive space analysis in three dimensions to assess maxillary growth.

Table 2. The Clinical Outcomes of Study Group and Control Group^a

	Study Group	Control Group
Bone volume	2.36 ± 0.35	2.57 ± 0.30
Impacted side for study group	Max: 33.5; Min: 18.3	Max: 36.6; Min: 22.4
Left side for control group		
Mean ± SD, 10 ⁴ mm ³		
Bone volume	2.37 ± 0.34	2.65 ± 0.38
Nonimpacted side for study group	Max: 34.2; Min: 18.6	Max: 31.4; Min: 21.2
Right side for control group		
Mean ± SD, 10 ⁴ mm ³		
Maxillary width, mm	64.3 ± 5.3	66.6 ± 3.6
	Max: 78.8; Min: 56.1	Max: 73.2; Min: 59.7
Maxillary height, mm	65.1 ± 3.6	67.0 ± 3.5
	Max: 70.0; Min: 55.0	Max: 74.6; Min: 59.7
Maxillary depth, mm	47.7 ± 3.6	49.6 ± 3.3
	Max: 55.5; Min: 41.2	Max: 56.4; Min: 40.7

^a SD indicates standard deviation; Min, minimum; and Max, maximum.

As a fundamental step in image data processing, identifying and delineating the anatomical structures of interest, known as image segmentation, has become a bottleneck step in the clinical application of 3D CBCT image analysis. Segmentation based on threshold values is simple and widely used, but it is nonspecific and artifact-prone.¹⁷ Additionally, there is a thresholding limitation, as a voxel is classified depending only on its intensity. It is, therefore, difficult to separate low-density or thin layer bone from the surrounding soft tissue.¹⁸ Cevidanes et al.¹¹ recommended ITK-SNAP software¹² for the segmentation procedures, which utilizes two active contour methods to compute feature images based on the CBCT image gray-level intensity and boundaries. However, the manual postprocessing takes several hours, becoming too tedious and time-consuming for practical and routine clinical application.

This study took one step forward by building the machine learning for automatic boundary recognition. The automatic segmentation method used was different from other automated segmentation methods (ie, ITK-SNAP,¹² which is mainly based on thresholding operation), as its algorithm includes shape information for robust segmentation and is less sensitive to the presence of artifacts commonly found in CBCT images.¹⁹ One advantage of this learning-based framework is that it can be applied to segment both normal and pathological subjects, in whom shapes often change significantly. Therefore, the maxilla in this study could be segmented based on a previously established training database for subjects with and without canine impaction. Another advantage of this proposed method is that it can be applied to CBCT images of varying quality, allowing for images with relatively poor quality that are challenging for manual segmentation to be segmented. Finally, the segmentation efficiency has been greatly improved using this fully automatic algorithm. The processing time for

segmentation of one set of CBCT images was significantly decreased to be 15 minutes, and the algorithm eliminated the need for manual postprocessing, moving closer to the requirements for clinical application.

Automatic methods for landmark selection and midsagittal plane (MSP) reconstruction can be utilized to identify additional landmarks for 3D cephalometric measurements. There are different methods to define the MSP for asymmetric assessment. In the future, there is a plan to investigate different MSPs and to increase the sample size to further validate and provide a method of image data processing for routine clinical implementation. For the most robust segmentation, additional layers of classifiers could also be included to obtain the optimal regions of interest.

CONCLUSIONS

- The average maxillary volume was smaller in the unilateral impacted canine SG than in the CG.
- Maxillary underdevelopment is more likely when unilateral canine impaction is present.
- The usefulness of palatal expansion for canine impaction patients may reside in the evidence of the machine learning data presented herein.

ACKNOWLEDGMENT

This study was supported, in part, by NIH/NIDCR R01DE022816 and Peking University Medicine Seed Fund for Interdisciplinary Research BMU2018MI013.

REFERENCES

1. Lee J-G, Jun S, Cho Y-W, et al. Deep learning in medical imaging: general overview. *Korean J Radiol.* 2017;18:570–584.
2. Baştanlar Y., Özuysal M. Introduction to Machine Learning. In: Yousef M., Allmer J. (eds) miRNomics: MicroRNA Biology

- and Computational Analysis. *Methods in Molecular Biology (Methods and Protocols)*. 2014;1107:105–28. Humana Press, Totowa, NJ
3. Yu X, Liu B, Pei Y, et al. Evaluation of facial attractiveness for patients with malocclusion: a machine-learning technique employing Procrustes. *Angle Orthod*. 2013;84:410–416.
 4. Ngan P, Hornbrook R, Weaver B. Early timely management of ectopically erupting maxillary canines. *Semin Orthod*. 2005;11:152–163.
 5. Cooke J, Wang H-L. Canine impactions: incidence and management. *Int J Periodontics Restor Dent*. 2006;26:483–491.
 6. Sajjani AK, King NM. Prevalence and characteristics of impacted maxillary canines in Southern Chinese children and adolescents. *J Investig Clin Dent*. 2014;5:38–44.
 7. Bedoya MM, Park JH. A review of the diagnosis and management of impacted maxillary canines. *J Am Dent Assoc*. 2009;140:1485–1493.
 8. Coulter J, Richardson A. Normal eruption of the maxillary canine quantified in three dimensions. *Eur J Orthod*. 1997; 19:171–183.
 9. Al-Khateeb S, Abu Alhajja ES, Rwaite A, et al. Dental arch parameters of the displacement and nondisplacement sides in subjects with unilateral palatal canine ectopia. *Angle Orthod*. 2012;83:259–265.
 10. Yan B, Sun Z, Fields H, et al. Etiologic factors for buccal and palatal maxillary canine impaction: a perspective based on cone-beam computed tomography analyses. *Am J Orthod Dentofacial Orthop*. 2013;143:527–534.
 11. Cevidanes LHC, Oliveira AEF, Grauer D, et al. Clinical application of 3D imaging for assessment of treatment outcomes. *Semin Orthod*. 2011;17:72–80.
 12. Yushkevich PA, Piven J, Hazlett HC, et al. User-guided 3D active contour segmentation of anatomical structures: significantly improved efficiency and reliability. *Neuroimage*. 2006;31:1116–1128.
 13. Wang L, Gao Y, Shi F, et al. Automated segmentation of dental CBCT image with prior-guided sequential random forests. *Med Phys*. 2016;43:336–346.
 14. Zhang J, Gao Y, Wang L, et al. Automatic craniomaxillofacial landmark digitization via segmentation-guided partially-joint regression forest model and multiscale statistical features. *IEEE Trans Biomed Eng*. 2016;63:1820–1829.
 15. O'Neill J. Maxillary expansion as an interceptive treatment for impacted canines. *Evid Based Dent*. 2010;11:86.
 16. Akhil G, Senthil Kumar KP, Raja S, et al. Three-dimensional assessment of facial asymmetry: a systematic review. *J Pharm Bioallied Sci*. 2015;7(suppl 2):S433–S437.
 17. Pham DL, Xu C, Prince JL. Current methods in medical image segmentation. *Annu Rev Biomed Eng*. 2000;2:315–337.
 18. Zhang J, Yan C-H, Chui C-K, et al. Fast segmentation of bone in CT images using 3D adaptive thresholding. *Comput Biol Med*. 2010;40:231–236.
 19. He L, Zheng S, Wang L. Integrating local distribution information with level set for boundary extraction. *J Vis Commun Image Represent*. 2010;21:343–354.